Chemical Engineering Journal 380 (2020) 122493

Contents lists available at ScienceDirect

Chemical Engineering Journal

journal homepage: www.elsevier.com/locate/cej

Multiplexed patterning of cesium lead halide perovskite nanocrystals by additive jet printing for efficient white light generation

Yemliha Altintas[a], Ilker Torun[b], Ahmet Faruk Yazici[a], Emre Beskazak[c], Talha Erdem[c], M. Serdar Onses[b,d,*], Evren Mutlugun[c,d,*]

[a] Department of Materials Science and Nanotechnology Engineering, Abdullah Gul University, Kayseri 38080, Turkey
[b] Department of Materials Science and Engineering, Nanotechnology Research Center (ERNAM) Erciyes University, Kayseri 38039, Turkey
[c] Department of Electrical and Electronics Engineering, Abdullah Gul University, Kayseri 38080, Turkey
[d] UNAM – Institute of Materials Science and Nanotechnology, Bilkent University, Ankara 06800, Turkey

HIGHLIGHTS

- Perovskite nanocrystals suffer from anion exchange reaction when mixed.
- E-jet printing of perovskite nanocrystals has been demonstrated.
- Superior white LED is achieved using perovskite nanocrystal stripes.

GRAPHICAL ABSTRACT

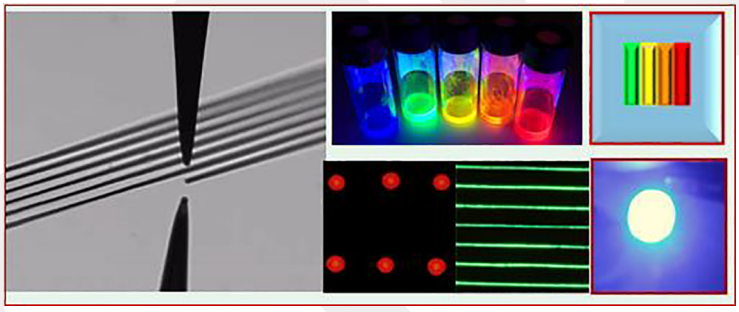

ARTICLE INFO

Keywords:
Perovskite nanocrystals
Anion exchange reaction
Electrohydrodynamic jet printing
White LED

ABSTRACT

Inorganic perovskite nanocrystals (PNCs) offer the ability to precisely but also flexibly control the peak emission wavelength while also possessing narrow-band emission spectra and high quantum yields. Owing to these features, PNCs have been already employed as color converters on LEDs. Nevertheless, the anion exchange reactions that prevent the blending of perovskites of different colors remain as an important bottleneck. As a remedy to this issue, here we employ additive jet printing to form separated stripes of these nanocrystals. Within this framework, we first present the synthesis of $CsPbBr_3$ and $CsPbBr_xI_{3-x}$ nanocrystals spanning the whole visible regime and optimize the cleaning procedure to obtain PNCs possessing photoluminescence quantum yields as high as 91% and emission linewidths as narrow as 15 nm, making them suitable for high quality white light generation. Next, we employ electrohydrodynamic jet printing to form closely spaced stripes of PNCs of various colors and integrated these films with a blue LED to create a white LED. Our proof-of-concept LED achieves high photometric performance as it possesses a color rendering index of 91.3, luminous efficacy of optical radiation > 300 lm/W_{opt}, and correlated color temperature of ca. 7000 K. We believe that additive jet printing technique will pave the way for a ubiquitous use of these PNCs in light-emitting devices in the near future.

* Corresponding authors at: Department of Electrical and Electronics Engineering, Abdullah Gul University, Kayseri 38080, Turkey (E. Mutlugun); Department of Materials Science and Engineering, Nanotechnology Research Center (ERNAM) Erciyes University, Kayseri 38039, Turkey (M. Serdar Onses).
E-mail addresses: onses@erciyes.edu.tr (M. Serdar Onses), evren.mutlugun@agu.edu.tr (E. Mutlugun).

https://doi.org/10.1016/j.cej.2019.122493
Received 27 May 2019; Received in revised form 30 July 2019; Accepted 12 August 2019
Available online 13 August 2019
1385-8947/

1. Introduction

Apart from the mature quantum dots of II-VI compounds of CdSe based or III-V InP based 0D nanocrystalline materials, perovskite nanocrystals (PNCs) are relatively a new subset of highly efficient emitters based on $CsPbX_3$ structure (X = Cl, Br, I) since their first demonstration in 2015 [1]. Their narrow emission bandwidth and tunable bandgap over the entire visible range make them important building blocks for colloidal optoelectronics [2]. Through the end use of these colloidal particles, display and lighting are amongst the main important application areas [3]. In this context, owing to their narrow full-width at half-maximum (FWHM) values, the color span of their color converted displays extends the National Television Standards Committee (NTSC) color gamut over 140% [1] and enable to achieve engineered white light with superior quality. There are early reports on InGaN blue LEDs hybridized with PNCs with up to 6-color-mixing (blue, cyan, green, yellow, orange, and red) which enables achieving color rendering indices > 90 by almost mimicking the sunlight [4]. The easiness in achieving full color spectra using an anion exchange reaction then allows for the precise determination of the peak emission wavelength [5]. However, although the green-emitting PNCs possess FHWM values of < 20 nm, the red-emitting PNCs have emission linewidths of ca. 40 nm which would decrease the overall color quality and efficiency of the white LEDs [6]. Thus, realizing narrower red-emitting PNCs is essential to achieve high quality displays and general lighting [6].

Creating a WLED by using color-converting semiconductor nanocrystals requires at least one red and one green component in addition to a blue LED chip that pumps the nanophosphors. Conventional II–VI or III–V semiconductor nanocrystals can be mixed in solution to create a down-conversion medium and generate white light under the excitation of a blue light source. PNCs emitting at different colors, on the other hand, are not suitable for blending to acquire white light spectrum although post-synthesis photoluminescence tunability of cesium lead halide perovskites by adjusting the halide ratios without any detrimental effect on the quantum yields has been shown [5,7]. This color shift is mainly due to anion exchange occurring between PNCs possessing different ion concentrations. Since the concentration of the anions defines the bandgap of a PNC, the diffusion of these ions causes the PNCs to possess the same bandgap causing emission in a single color rather than the combination of different colors creating the white light emission. For example, $CsPbX_3$ nanocrystals (X = Cl, Br, I) emitting in different colors possess yellow emission spectra when mixed, rather than preserving their individual green and red emission colors.

In order to utilize PNCs in down-conversion WLEDs, numerous methods have been proposed. One way is to hybridize red emitting PNCs with green-yellow phosphors to improve low CRI caused by inefficient red phosphors. Using this approach, Zhou et al. reported a correlated color temperature (CCT) of 4222 K and a color rendering index (CRI) of 92 by using alloyed $CsPbBr_{1.2}I_{1.8}$ and YAG phosphors while the bare YAG-LED exhibited a CRI of 74 at a CCT of 6713 K [8]. Likewise, Song et al. modified polymer film compounds and improved quantum yield of PNC films leading to a tunable CCT ranging from 3897 K to 4758 K while CRI could be controlled between 90.3 and 95.1 [9]. Conversely, hybridization of green-emitting PNCs with a red-emitting phosphor resulted in a color gamut of 121% of the NTSC standard color gamut showing the suitability of these materials for display applications [10]. Furthermore, red and green PNCs were separately embedded in polymer matrices to create free-standing films and laminated on top of commercial blue LEDs. The white LED prepared by Pathak et al. using this method reached a CRI of 86 and a CCT of 5229 K by replacing phosphors with PNCs [11]. Another approach on using PNCs in WLED applications is to employ a mesoporous silica coating that prevents the anion exchange reaction between PNCs with different compositions. Di et al. used this method to construct a WLED with a CCT of 4718 K and a CRI of 92 yet this method creates local agglomerations which causes a 20–50% increase in FWHM [12]. Similarly, Shao et al. prepared $CsPbX@SiO_2$ composites and mixed with PMMA to create a down-conversion coating and achieved a CRI of 91 and a CCT of 5218 K [13]. Nevertheless, it remains an unmet challenge to fabricate WLEDs by the direct use of PNCs without needing any additional encapsulation processes that would also inhibit the ion exchange in the hybrid film.

To address the challenge of physically confining different colors of PNCs in a certain volume, here we introduce additive jet printing as an approach to enable direct delivery of materials with high levels of registration and resolution that offers the possibility to position and pattern multiple materials without any cross-contamination. A particularly interesting technology is electrohydrodynamic jet (e-jet) printing, which relies on electrohydrodynamically induced flow of materials from nozzles allowing for additive patterning of different materials [14–16]. Besides the advantages in the lateral resolution, e-jet printing provides precise control over the thickness of the printed films and improved registration based on focusing of the electric field [17,18]. Previous research demonstrated practical utility of this approach for patterning colloidal nanoparticles to fabricate plasmonic circuits [19] and LEDs [20]. In this work, we utilized the afore-mentioned strengths of e-jet printing to create color-converting films for obtaining a high quality white LED. To achieve this, we first optimized our PNC synthesis and obtained PNCs possessing fluorescence quantum yields > 90% and FWHM values < 20 nm. By employing these PNCs, we printed green-, yellow-, orange-, and red-emitting PNC stripes and hybridized them with a blue LED to realize a white LED. Our final device exhibited a CRI of 91.3, an LER of 300 lm/W_{opt}, and a CCT of 7000 K indicating successful color rendition capability, good overlap with the human eye sensitivity function, and a cool white shade.

To the best of our knowledge, engineering the specifications of white light through additive printing of materials with different emissive properties without deteriorating the original emission color of PNCs has not been reported before. We believe that this first demonstration of e-jet printing of PNCs also offers novel routes for device level integration of these interesting materials. In addition, we introduce the optimization of the post synthesis processing routes in order to control the emission bandwidth of the red emitting PNCs allowing to reach red emitting PNCs as narrow as 30 nm.

2. Experimental

2.1. Synthesis of Cs-based inorganic PNCs

PNCs were synthesized according to the previous reports [1,21,22] with minor modifications.

2.1.1. Preparation of the Cs-oleate

This precursor was prepared in three-neck flask by mixing Cs_2CO_3 (0.407 g), octadecene (ODE) (20 mL), and oleic acid (OA) (1.55 mL). This mixture was heated to 120 °C under vacuum for 60 min. Subsequently, the temperature was increased to 150 °C under argon atmosphere and the mixture was kept at this temperature until all Cs_2CO_3 completely dissolved in ODE. After cooling down at room temperature, this solution was stored inside the glovebox.

2.1.2. Green-emitting PNCs synthesis

0.57 mmol of $PbBr_2$ and 12 mL of octadecene (ODE) were mixed in a 25 mL three-necked flask for 30 min under vacuum with strong agitation. After three cycles of evacuation and gas flushing, the temperature of the solution was increased to 120 °C under argon atmosphere. Next, 1.5 mL of oleylamine (OLA) and 1.5 mL of OA were injected into the flask at 120 °C. After the injection of these precursors, the solution became transparent. Then, the temperature was increased to 170 °C and 1.2 mL stock solution of Cs-oleate was quickly injected into the flask, and the solution was quickly cooled down to room temperature using cold water. To purify the PNCs, as-synthesized nanocrystals were

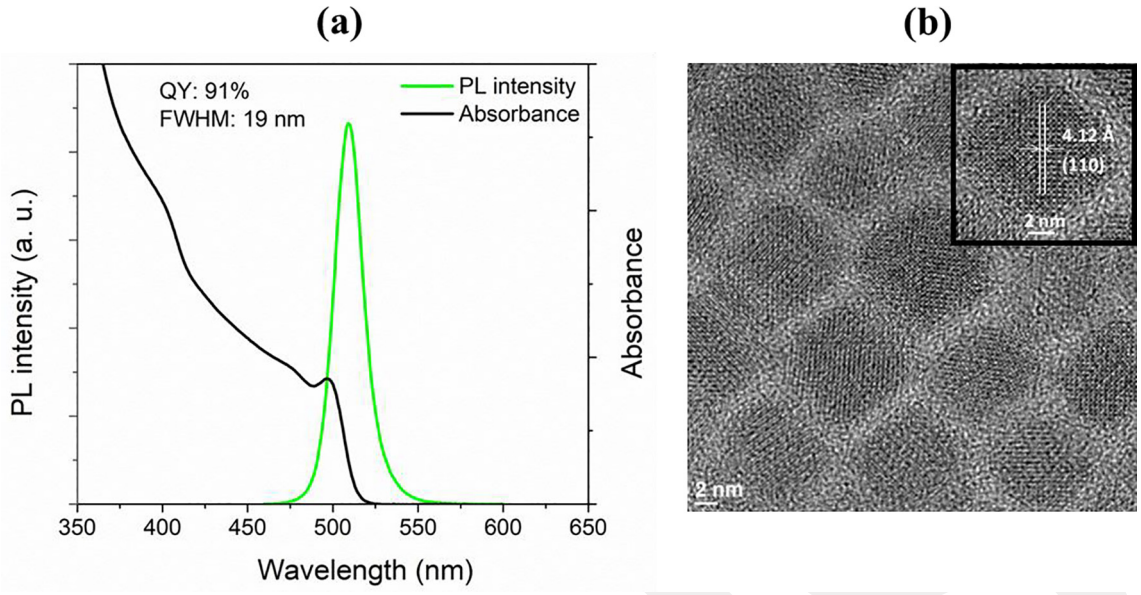

Fig. 1. (a) Photoluminescence and absorbance spectra of the green-emitting $CsPbBr_3$ PNCs and their (b) HR-TEM image (inset image shows d-space of a PNC). (For interpretation of the references to color in this figure legend, the reader is referred to the web version of this article.)

centrifuged at 5000 rpm for 6 min using three centrifuge tubes each having a volume of 15 mL. After the supernatant was discarded, a small volume of hexane (0.4 mL) was added to each centrifuge tube and the precipitate was dispersed. The PNC solution was centrifuged once more (5000 rpm, 6 min) to remove large and agglomerated nanoparticles. This time the precipitate was discarded, and the supernatant was collected. Next, 0.4 mL of hexane, 30 μL of OLA and 30 μL of OA were added to each centrifuge tube. Again, the solutions were centrifuged at 5000 rpm for 4 min and precipitates were dissolved in hexane.

2.1.3. Measurement of quantum yield

The quantum yield (QY) of the samples has been measured by comparing with an organic dye using the methodology explained and given in the literature [23–25].

2.2. Anion exchange reaction in Cs-based inorganic PNCs

Anion-exchange reactions of Cs-based PNCs were performed by using nanocubes of PNC in glovebox following the previously reported recipe [26]. First, $PbCl_2$ and PbI_2 containing anion-exchange solutions were prepared separately by mixing 5 mL of hexane, 0.2 mmol PbX_2 ($PbCl_2$ or PbI_2), 0.2 mL of OA, and 0.25 mL of OLA. Until all PbX_2 (X: Cl or I) dissolved in solution, the solutions were stirred at 50–55 °C in 20 mL vial and stored in glovebox. Second, 0.15 mL of cleaned green PNCs were placed in a vial and mixed with the desired amount of anion exchange solution which determines the final emission wavelength of the PNCs. The yellow-, orange-, and red-emitting PNCs were obtained by treating (150 μL) of the green-emitting PNCs having 24 mg/mL concentration with PbI_2 containing anion exchange solution (150 μL, 200 μL and 300 μL for yellow-, orange-, and red-emitting PNCs, respectively). Blue-emitting PNCs were synthesized by treating the green PNCs with 150 μL of $PbCl_2$ containing anion exchange solution. Finally, anion-exchanged PNCs were cleaned with ODE (by varying the ODE concentration from 0.5 to 2.0 mL) and ethyl acetate (4 mL) to obtain a high QY.

2.3. Electrohydrodynamic jet printing of perovskite nanocrystals

Silicon wafers (<1 0 0>, Wafer World Inc.) and glass slides (Isolab Inc.) were cut into square pieces (2 × 2 cm^2) with a scriber. The substrates were sequentially cleaned in acetone and ethanol for 5 min under sonication and then dried with nitrogen. An additional cleaning was performed prior to the printing via UV-Ozone treatment for 20 min. In the case of hydrophobic substrates, a film was deposited from vapor phase on the freshly cleaned substrates. For this purpose, the substrate was placed in a closed container along with a droplet (10 μL) of tridecafluoro-1,1,2,2-tetrahydrooctyl-trichlorosilane (Gelest Inc.) under ambient conditions for 10 s.

E-jet printing was performed via a customized desktop setup that consisted of a motorized stage synchronized with a voltage supplier. Hardware details of the e-jet printing system can be found in the literature [27]. High-resolution printing was performed using pre-pulled glass pipettes (World Precision Instruments) with inner nozzle diameters of 1 μm, 5 μm and 10 μm. A film (~50 nm) of gold was evaporated on the glass pipettes to generate a conductive path. Arrays of PNCs for white-light generation were fabricated using steel nozzles (Fhis Electronic Inc.) with an inner diameter of 60 μm. The working distance between the tip of the nozzle and substrate was set at 80 μm through optical imaging. The ejection of the droplets was performed via application of a voltage bias between the nozzle and grounded substrate. In the case of high-resolution printing experiments using fine nozzles, the applied voltage was ~350 V. The fabrication of white light emitting diode was performed with a voltage of ~700 V. The spatial position of the droplets was defined by the controlled movement of the substrate with the motorized stage. The ink composed of PNCs suspended in hexane at a concentration of 25 mg/mL. In the case of fabrication of white light emitter, as-synthesized and anion-exchanged PNCs were used without any dilution. The ink was diluted (1:4) with addition of hexane for high resolution printing experiments using nozzles with inner diameters of 5 μm and 1 μm.

2.4. Characterizations

Optical characterizations of synthesized PNCs such as photoluminescence and absorbance were carried out by using Agilent-Cary Eclipse fluorescence spectrophotometer and Thermo Genesys 10S UV–Vis spectrometer, respectively. In order to perform X-ray diffraction and time correlated single photon counting (TCSPC) measurements, PANalytical: X'pert Pro MPD and Pico Quant FluoTime 200 (equipped with 375 nm pulsed laser diode) have been used. TEM images and EDX-measurements of the synthesized nanocrystals have been performed by using FEI Tecnai G2 F30 (equipped with Energy Dispersive X-ray

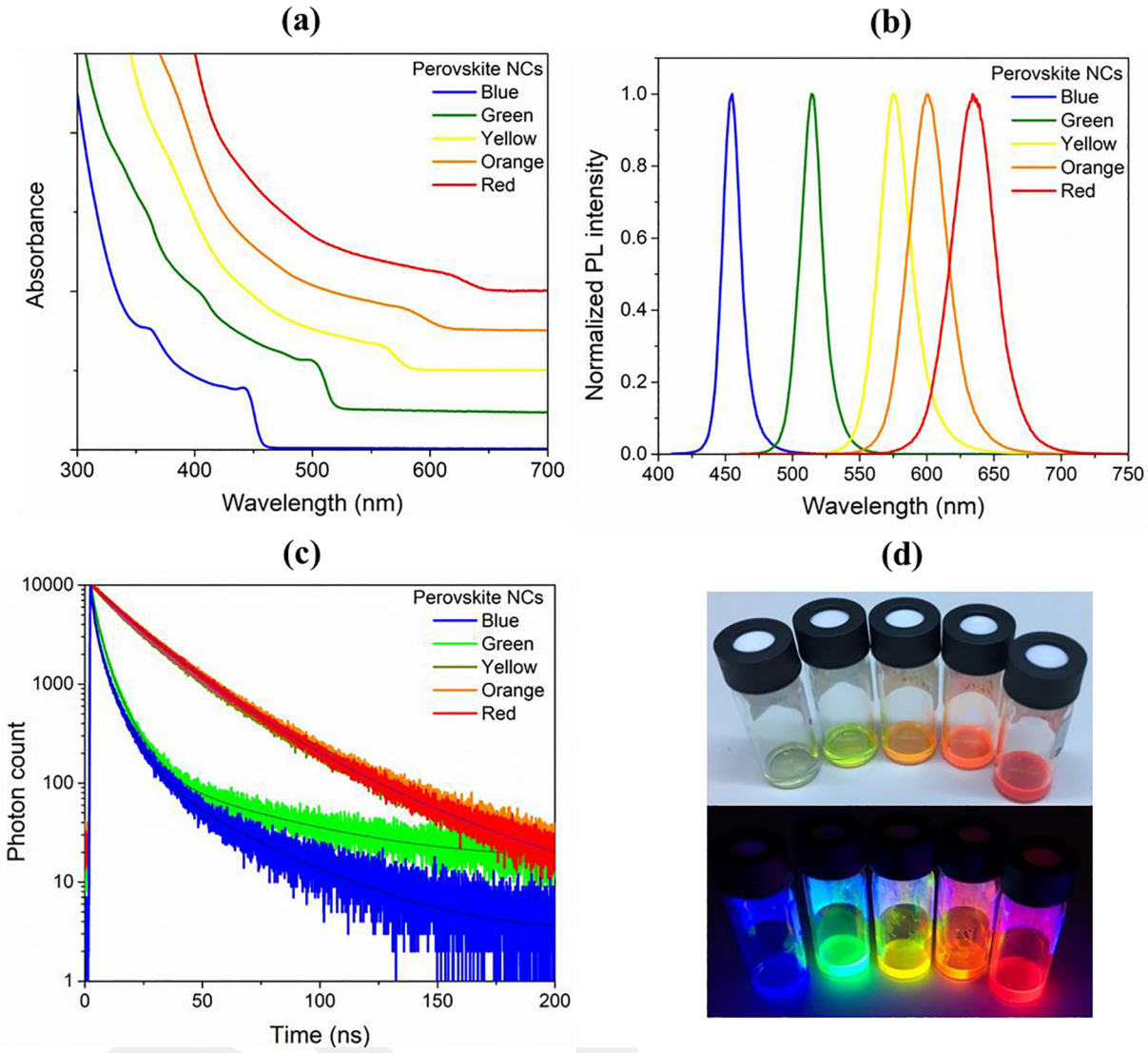

Fig. 2. (a) Absorbance, (b) photoluminescence and (c) TRF measurements of the synthesized PNCs by using anion exchange reaction. (d) Real color photos of the synthesized samples with and without UV illumination.

Table 1
Optical properties of used green PNCs and as-synthesized anion-exchanged samples.

	Peak emission wavelength (nm)	PL QY (%)	FWHM (nm)	$\tau_{average}$ (ns) (amplitude weighted)
Seed-Green PNCs	514	91	19	5.44
After anion-exchance reaction				
Yellow	575	81	27	20.73
Orange	600	77	33	22.93
Red	634	84	37	22.54
Blue	455	81	15	4.88

spectroscopy (EDAX)).

The static contact angle of the substrates and thickness of vapor deposited fluoroalkyltrichlorosilanes were measured via a contact angle meter (Attension Theta Lite system) and a stokes ellipsometer (Gaertner), respectively. The height profiles of the printed linear features were obtained by employing an AFM (Veeco Multimode 8) operated in tapping mode. The morphology of the patterned nanocrystals was obtained at 25 kV via a SEM (Zeiss EVO LS10). Optical microscopy images were acquired using a light microscope (Leica DM750M). The localized photoluminescence from patterned PNCs was characterized via a fluorescence microscope (Olympus BX43 Tokyo, Japan equipped with a DP73 digital camera). White LED was fabricated using a commercially available InGaN LED, with PNCs hybridized on it, and driven with Keithley 2400 source meter. The photoluminescence emission spectra were collected using an Ocean Optics QE Pro spectrometer. Stability test of the device was performed immediately after the device fabrication to eliminate the degradation of PNC materials. The glass substrate on which the device is fabricated was placed on commercial InGaN blue-LED and photoluminescence spectra was collected with Ocean Optics QE Pro spectrometer. The electroluminescence spectra were collected in 5-minute intervals. The first measurement was accepted as the initial state of the device and shown in Fig. S7 as t = 0.

The luminous flux of our device as a function of current using an integrating sphere is presented in Fig. S6. Luminous flux data was collected using Hamamatsu C9920-12 EQE measurement system. The PNC-LED device excited by a commercial blue LED and placed in the integrating sphere. The data was recorded by running the device from 0 to 3 mA using Keithley 2400 source meter.

Photoluminescence quantum yield (PLQY) measurement of the solid film was carried out using a commercially available blue LED as the excitation source. First, the blue LED spectrum was collected by

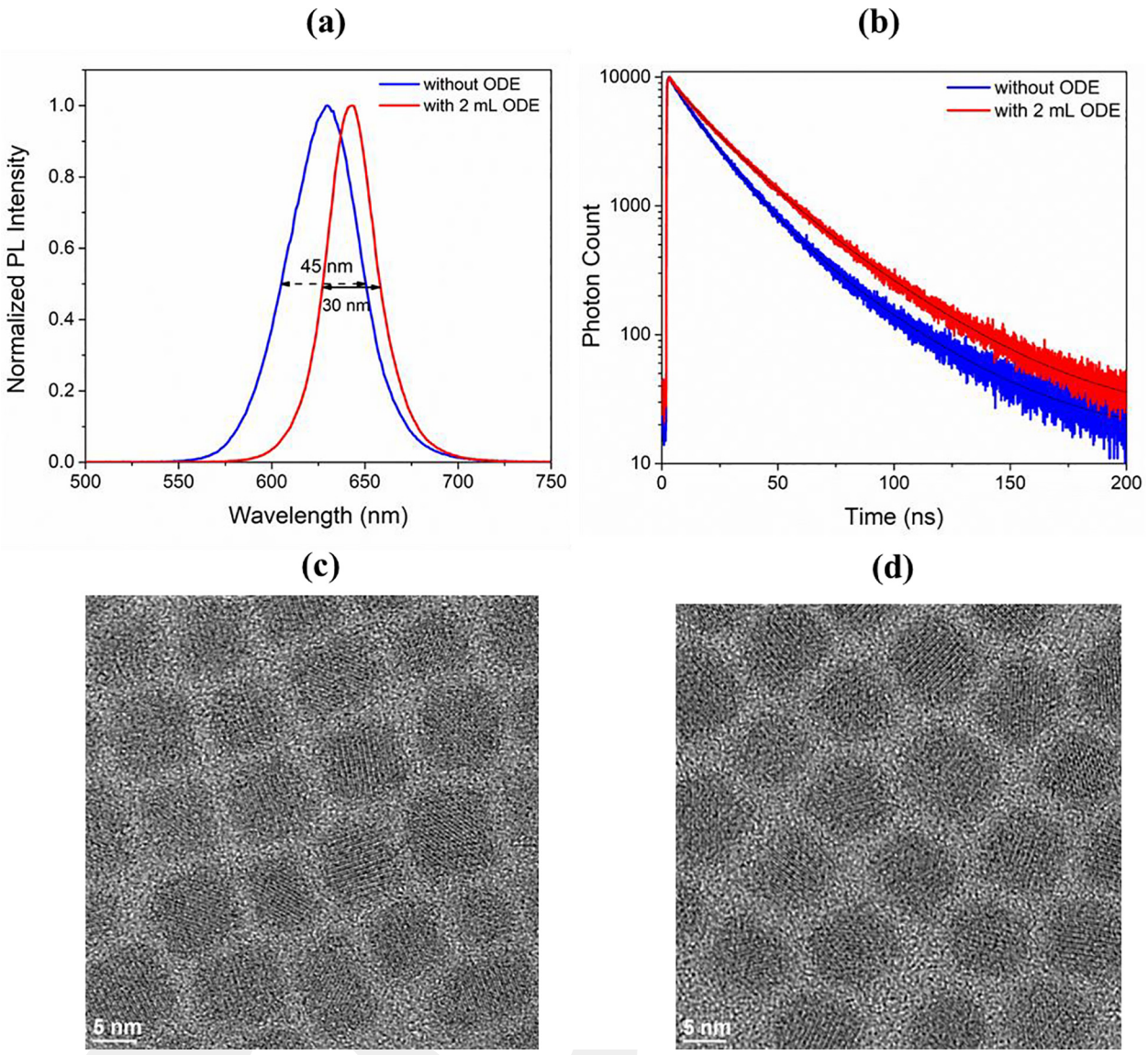

Fig. 3. (a) Photoluminescence, (b) time resolved photoluminescence spectra of the red-emitting PNCs cleaned without and with 2 mL of ODE after anion exchange reaction. FWHM of the sample cleaned using ODE decreased by 15 nm. TEM images of the samples cleaned (c) without ODE and (d) with 2 mL of ODE. (For interpretation of the references to color in this figure legend, the reader is referred to the web version of this article.)

employing the integrating sphere of Hamamatsu C9920-12 EQE measurement system. Next, the glass slide on which PNC LED is fabricated was placed on top of the LED and the resulting spectrum under the same experimental conditions was recorded. The difference between the integrals of the blue portion of spectra gives total number of absorbed blue photons. The total number of photons emitted by the PNC film was found by taking the integral of the PNC-LED spectrum in the interval of PNC emission range.

3. Results and discussion

The emission colors of Cs-based PNCs can be tuned from deep-blue region to red by controlling the concentrations of individual anions, such as chloride, bromide, and iodide (Cl_xBr_{3-x} and Br_xI_{3-x}). Nevertheless, due to the nature of its ion containing structure, preserving optical properties of the PNCs is not possible when the medium contains halide ions. It is also not applicable to use PNCs possessing different ion concentrations (i.e., PNCs emitting different colors) together due to exchange of these ions. Because the anion exchange reaction occurs at any temperature, the color of the PNCs degrades easily, even with the addition of any solvent and increasing the temperature. We showed this effect by only mixing red- and green-emitting PNCs without any additional chemicals (see Fig. S1). Upon addition of red-emitting PNCs, the peak emission wavelength of the green-emitting PNCs shifted from 514 nm to 589 nm due to the anion exchange (Fig. S1 and Table S1). Although this variation in the optical properties is a big hindrance against using PNCs of different colors together, which limits their application in general lighting and display backlighting, controlling the anion exchange also offers precise spectral tuning. To enable the simultaneous use of PNCs emitting different colors, here we propose e-jet printing that allows for creating spatial distance between stripes of PNCs and avoids the anion exchange.

The optical properties of PNCs via anion exchange reaction mostly depend on the starting green emitting PNCs. To achieve high efficiency yellow-, orange-, and red-emitting PNCs using anion exchange, we first synthesized high quality green-emissive PNCs. At this point, it is worth highlighting that obtaining highly emissive PNCs strongly depends on the cleaning procedure of the PNCs as explained in detail in the Section 2. By following the optimized procedure, we could obtain high quality pure green-emitting PNCs which have a QY of 91%, a peak emission

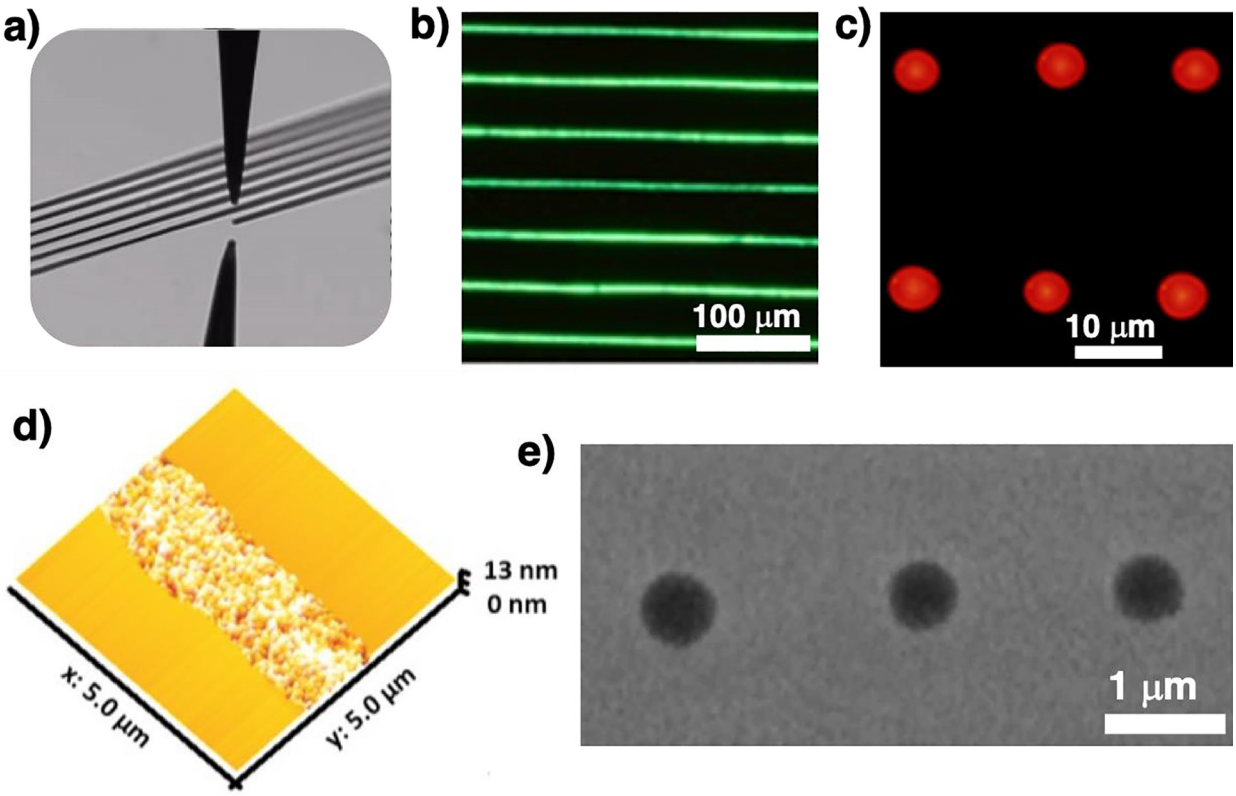

Fig. 4. E-jet printing of PNCs. a) A snapshot taken during the printing of PNCs via a tilted optical imaging system integrated to the printer setup. Shown is the nozzle and its mirror image, which is a reflection from the substrate. b, c) Fluorescence microscope image of printed arrays of lines and dots. The inks consisted of b) $CsPbBr_3$, and c) anion-exchanged $CsPbI_3$. d) An AFM image of a line printed at a stage speed of 50 mm/s using an ink of $CsPbBr_3$ diluted with hexane. e) SEM images of sub-micron dots printed using a nozzle with an inner diameter of 1 μm. The ink consisted of $CsPbI_3$ diluted with hexane. All substrates were hydrophobized with a film of fluoroalkyltrichlorosilanes.

wavelength at 514 nm, and a FWHM of 19 nm (Fig. 1a). The TEM image of the synthesized green-emitting PNCs shows that our nanocrystals possess a cubic form with sizes around 8 nm (Fig. 1b). d-spacing between two sequential plane of the cubic phase $CsPbBr_3$ PNCs have been measured from HRTEM image of the PNCs as shown in Fig. 1b as 0.412 nm that corresponds to the (1 1 0) crystal plane. Elemental analysis of the $CsPbBr_3$ NCs has been collected from TEM-measurements and individual elements of the PNCs in their structure have been shown in Fig. S2 and measured atomic percentages of the elements have been presented as an inset in the figure.

By systematically tuning the anion exchange reaction, as provided in the Section 2, we were able to synthesize efficient PNCs spanning the visible spectrum from blue to red (Fig. 2). Absorbance and PL spectra of the samples used in anion exchange reaction are presented in Fig. 2a and b. In the absorption spectra, we reckon that the blue-emitting and green-emitting PNCs possess sharp exciton peaks whereas the yellow-, orange-, and red-emitting PNCs have smoother exciton peaks. When we take a look at the photoluminescence spectra, we realize that blue- and green-emitting PNCs have FWHMs narrower than 20 nm while the emission linewidths of other PNCs are broader (Table 1). These are attributed to the inhomogeneity of the chemical composition in the PNCs after anion-exchange using PbI_2. It is also apparent that the anion exchange reaction decreases the quantum yield of the PNCs from 91% to around 80% regardless of the type of anion that we employ. Time resolved fluorescence (TRF) measurements shown in Fig. 2c indicate that the lifetime of the emitter lengthens with the increasing iodide concentration from 5.44 ns to 22.93 ns, while the lifetime shortens with the addition of the chloride containing solution from 5.44 ns to 4.88 ns. The detailed analysis of the TRF results including the fitting parameters is given in Table S2.

PLQY of the blue emissive PNCs synthesized by direct synthesis is generally lower than green and red emissive PNCs. Anion exchange reaction is the way to get high quality blue emissive PNCs which have been also reported recently [28]. For achieving high quality lighting the ability to control the optical features of the nanophosphors is very important [29]. It has been shown that especially the linewidth of the red color component has to be selected as narrow as possible [30]. To obtain red-emitting Cs-based PNCs with a narrow emission bandwidth, we investigated the effect of the ODE in anion exchange reaction. Narrower FWHM values of the emitters were achieved with the addition of ODE due to the effect of the size or compositional selective precipitation. Subsequently, we studied the effect of ODE during the cleaning procedure by increasing its volume up to 2 mL. We showed that emission linewidths of the samples decreased from 45 nm to 30 nm when ODE was introduced during the cleaning step (Figs. S3 and 3) accompanied by prolonged fluorescence lifetime from 19.16 to 24.12 ns (Fig. 3, Tables S3 and S4). EDX analysis of the samples, which were cleaned with and without addition of ODE after anion exchange reaction, has been presented in Table S5. XRD patterns of the synthesized $CsPbBr_3$ PNCs and anion exchanged $CsPbI_xBr_{3-x}$ PNCs have been presented with their related diffraction planes and the reference PDF cards in Fig. S4. Due to the hybrid structure of the $CsPbI_xBr_{3-x}$ PNCs, XRD peaks of the $CsPbI_xBr_{3-x}$ PNCs locate between the $CsPbBr_3$ PNCs and $CsPbI_3$ PNCs. After anion exchange reaction, it can be clearly seen that the structure of $CsPbBr_3$ PNCs changed from $CsPbBr_3$ PNCs to $CsPbI_xBr_{3-x}$ PNCs. The peak shifts in XRD pattern to the smaller 2-Θ values proves this structural change of the PNCs via anion exchange reaction. During the anion-exchange process, some part of the seed nanocrystals complete this exchange process, while the rest do not. Therefore, the solution has different compositions of nanocrystals which results in broader FWHM and inhomogeneous broadening in PL spectra. After centrifugation, the precipitate consists of heavier

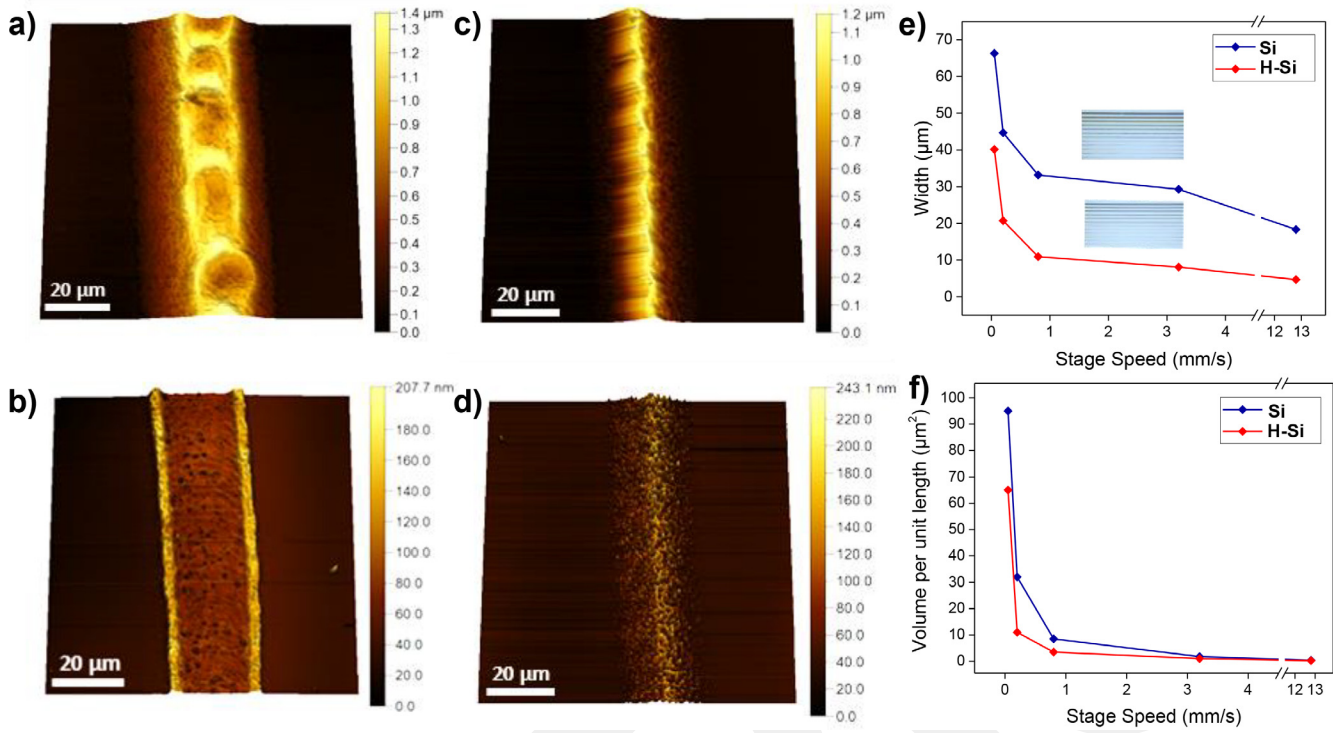

Fig. 5. The effect of stage speed and substrate wetting properties on the dimensions and morphology of the printed features. a–d) AFM images of lines on a, b) freshly cleaned silicon and c, d) hydrophobic substrates printed at a speed of a, c) 0.2 mm/s, b, d) 3.2 mm/s. e) The width of the printed lines as a function of the stage speed on a freshly cleaned silicon (Si) and hydrophobized silicon (H-Si) substrate. The insets show optical microscope images of an array of lines defined at different stage speeds. f) The volume per unit length as a function of the stage speed, as determined from the area under the height profile obtained from a line-section perpendicular to the long axis of the printed line. The inner diameter of the nozzle was 10 µm.

nanocrystals and size distribution or composition of the precipitated nanocrystals is nearly the same which result in narrower FWHM. Precipitated nanocrystals are dissolved in hexane and colorful supernatant is discarded. Narrower FWHM can be achieved with size or compositional selective precipitation method by using ODE during the centrifuge process.

These results suggest that ODE contributes to preserve the chemical composition, helps selective precipitation, avoids the aggregation of the particles, and also narrows their emission linewidths.

Device applications that range from light emitting diodes to lasers require spatially defined placement of solution synthesized PNCs onto solid substrates. Here, we demonstrate one-step direct patterning of multiple PNCs using electrohydrodynamic jet (e-jet) printing (Fig. 4). Electric fields applied in between a conductive nozzle and substrate results in ejection of inks that consist of PNCs dissolved in hexane (Fig. 4a). The application of electric field leads to the build-up of ions at the tip of the nozzle near the meniscus. When the strength of the electric field and associated electrostatic stresses are stronger than the surface tension, the material is ejected from the nozzle [14]. In the case of nozzles with inner diameters of 1 µm and 5 µm, the concentration of PNCs was reduced by addition of hexane for smooth printing operation. As-synthesized and anion-exchanged PNCs could be printed in linear and dot geometries with intense and localized photoluminescence from the patterns (Fig. 4b, c). A key advantage of e-jet printing is its completely additive nature allowing direct delivery of PNCs overcoming the need for multiple processing steps that may contaminate both the PNCs and substrates resulting in loss of intensity and specificity of photoluminescence from the patterned arrays. The use of fine nozzles together with proper choice of printing conditions (i.e. stage speed, voltage) enable high-resolution patterning of linear and dot features with critical dimensions on the order of a micrometer (Fig. 4d, e). Previous studies [15,18], have shown that features with critical dimensions that are smaller than 100 nm can be patterned with e-jet printing. Further engineering the composition of inks together with the use of fine nozzles can enable nanoscale patterning of PNCs. The height of the printed features can be reduced leading to a quasi-monolayer of PNCs.

Fig. 5 presents the capabilities of e-jet printing in controlling the lateral and out of plane dimensions of the patterns of PNCs. For a fixed ink composition and strength of electric field defined by the voltage bias and working distance, the width, height and morphology of the linear features depend on the translational speed and wetting property of the substrate. Fig. 5a, b, for example, present AFM images of such linear patterns printed on a freshly cleaned silicon substrate at stage speeds of 0.2 mm/s and 3.2 mm/s, respectively. The build-up of material at low stage speeds results in increase of the height of the line together with in-plane spreading. At high stage speeds on the freshly cleaned silicon substrate, the edges of the printed lines were significantly higher than the center, as a result of a phenomenon commonly referred as the coffee-ring effect. The wetting property of the substrate also plays a critical role (Fig. 5c, d). We deposited a film of fluoroalkyltrichlorosilanes to reduce the surface energy of the substrate [31]. After the deposition of ~2 nm of fluoroalkyltrichlorosilanes, the initially hydrophilic silicon wafer became hydrophobic with a static water contact angle of ~105°. The extent of spreading was limited with the fluoroalkyltrichlorosilane treatment and the line widths were consistently lower in comparison to bare silicon substrate for a range of stage speeds (Fig. 5e). The center of the lines printed on the hydrophobic substrate was higher than the edges showing that the coffee-ring effect is suppressed, which is likely a result of the de-pinning of the contact line on this type of substrate. Overall the width of the lines and printed volume of material per unit length scaled inversely with the stage speed as consistent with the past studies [15,17].

To study the potential of our PNCs as color-convertors, we also prepared their white LEDs. Prior to e-jet printed LEDs, we first

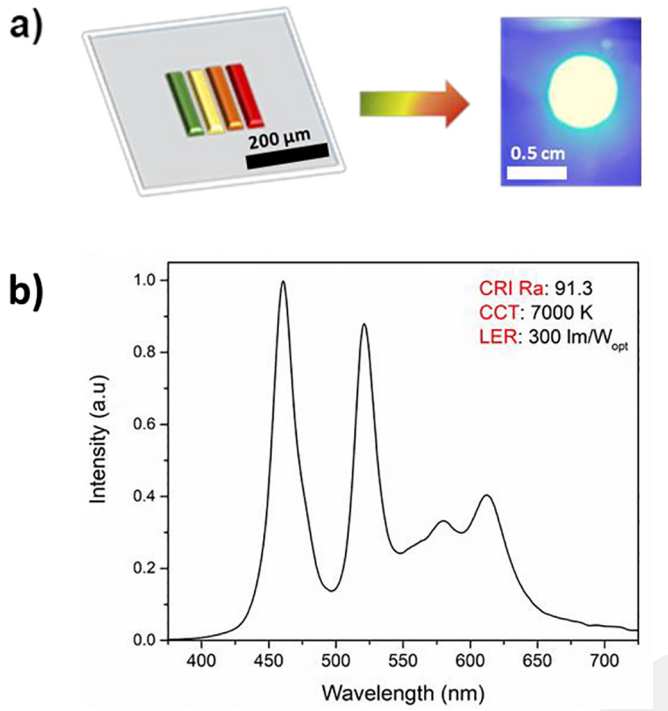

Fig. 6. Printing multi-color emitting PNCs for fabrication of white light-emitting devices. a) Schematic description of the printing linear arrays of green, yellow, orange and red emitting PNCs. Printing was performed at a speed of 0.1 mm/s on an ITO-coated glass substrate using a nozzle with an inner diameter of 60 µm. The working distance between the tip of the nozzle and substrate was set as 200 µm. Each PNC was printed to fill an area of 0.85 × 5 mm^2. The substrate was placed on top of a blue-emitting LED chip to generate the white light shown in the picture along with an inset showing the printed arrays. b) Spectrum of the printed arrays of PNCs under excitation with the blue emitting LED. (For interpretation of the references to color in this figure legend, the reader is referred to the web version of this article.)

employed their individually drop-cast PNC films on a blue LED to evaluate the photometric performance of the white LEDs. Similar to previous reports [30,32] on white LEDs of colloidal quantum dots, we designed several four-colors-LEDs made of green-, yellow-, and red-emitting PNCs on a blue LED. The resulting performance reported in Fig. S5 shows that these four-colors-LEDs may possess a good spectral overlap with the human eye sensitivity function as the luminous efficacy of optical radiation (LER) values ~325 lm/W$_{opt}$ indicate. Nevertheless, achieving superior color rendition is problematic as all the four-color LEDs have CRIs < 90. To improve this performance, we added orange-emitting PNC films as the fifth color component to our LEDs. Results show that CRIs > 91 together with LERs > 300 lm/W$_{opt}$ can be achieved with this configuration. We also studied whether these PNCs can potentially be suitable for display applications by calculating the color gamut attainable with these LEDs and comparing it with the NTSC gamut. As shown in Fig. S5b, these white LEDs are able to reach color gamuts greater than the NTSC color gamut, proving their potential for display applications.

After proving the potential of our PNCs with individually drop-cast films, we fabricated a five-colors-white LED using e-jet printing method. The additive nature of e-jet printing allows for well-registered patterning of multiple materials across a single substrate. Based on this capability, we fabricated printed pads (250 µm × 1 mm) of PNCs that emit light in a range from 520 nm to 630 nm (Fig. 6a). Green, yellow, orange and red emitting PNCs were sequentially printed using different nozzles with the same single-nozzle print head. Previous research [33] has shown e-jet printing of multiple materials using multi-nozzle print heads. The spacing in between the patterns of different PNCs was kept at ~20 µm that is sufficient to prevent mixing and anion exchange between PNCs. The spatial borders of PNC lines have been defined with e-jet and the amount of PNCs have been optimized to suppress the underlying blue LED emission. The achieved five-color white LED generates a cool white light as its correlated color temperature of 7000 K shows while successfully rendering the real colors of the objects as indicated by its CRI of 91.3. Furthermore, the LER of this LED achieved ~300 lm/W$_{opt}$ indicating a moderate overlap with the human eye sensitivity function of the emitted light.

Here, it is worth noting that white LEDs of colloidal nanomaterials usually employ either a blend of nanoparticles or their layered films. In both of the cases; however, the reabsorption of the light generated by short-wavelength-emitting nanocrystals by the longer-wavelength-emitting PNCs inevitably decreases the overall efficiency [34]. Moreover, in the case of the films made of nanocrystal blends, the Förster-type energy transfer further reduces the overall efficiency. Different than these conventional methods, e-jet printing that we utilized in this work poses an important advantage. It enables the placement of different types of nanocrystals side-by-side and far away from each other, which reduces the negative effects of energy down-conversion and nonradiative energy transfer potentially leading to higher efficiencies. The devices were fabricated as a hybridized color converter on inorganic light emitting diodes. Since the light emission mechanism of PNCs in our device does not rely on charge injection but actually occurs due to color conversion, the internal and external quantum yields of the device are heavily dependent on the performance of the blue LED chip we employed. Because the blue LED chip does not reflect the real features of our materials, we believe that it would be more appropriate to include the photoluminescence quantum efficiency of our PNC-film.

The ratio of the emitted number of photons to the number of the absorbed blue photons gives the external quantum efficiency value, which turned out to be 6.5%. We have further carried out the operational stability test of our devices. For this purpose, we evaluated the variation of the total intensity and the color rendition performance of the final device (Fig. S7 and S8). The total integrated intensity plot indicates that our PNC color converters possess a reasonable stability and retains > 50% of their initial intensity for 12 h even though no encapsulation has been employed at all.

4. Conclusions

In conclusion, here we showed that the anion exchange enables tuning the emission color of the cesium lead halide based PNCs throughout the whole visible spectrum. Furthermore, we for the first time showed that the inclusion of ODE during the cleaning process significantly decreases their emission linewidths by 15 nm. We believe that this additional ODE avoids the aggregation of the nanocrystals, passivates their surface, and helps to maintain a stable chemical composition distribution among the synthesized colloidal PNCs. Here, we also proposed e-jet printing of these nanocrystals that will enable the collective use of PNCs having different colors on optoelectronic devices and avoid the anion exchange reactions in a film of nanocrystal blends. This technique enabled us to form spatially separated controllable patterns of PNCs having different emission colors. Finally, we integrated these printed films composed of PNC stripes emitting in four different colors with a blue LED. Our white LED possessed a color rendering index of 91.3, a luminous efficacy of optical radiation of ~300 lm/W$_{opt}$, and a correlated color temperature of 7000 K simultaneously, indicating its superior photometric efficiency and high color quality. Without any encapsulation, the total integrated intensity indicates that our PNC color converters possess a reasonable stability and retains > 50% of their initial intensity for 12 h. We believe that the results presented here may open up new possibilities for the perovskite-based lighting and display systems.

Acknowledgments

We acknowledge TUBITAK, Turkey, project no. 117E239 and also partial support from the Turkish Academy of Sciences Distinguished Young Scientist Award (TUBA-GEBIP).

Appendix A. Supplementary data

Supplementary data to this article can be found online at https://doi.org/10.1016/j.cej.2019.122493.

References

[1] L. Protesescu, S. Yakunin, M.I. Bodnarchuk, F. Krieg, R. Caputo, C.H. Hendon, R.X. Yang, A. Walsh, M.V. Kovalenko, Nanocrystals of cesium lead halide perovskites (CsPbX < inf > 3 < /inf > , X = Cl, Br, and I): novel optoelectronic materials showing bright emission with wide color gamut, Nano Lett. 15 (2015) 3692–3696, https://doi.org/10.1021/nl5048779.

[2] Y. Dong, Y. Zhao, S. Zhang, Y. Dai, L. Liu, Y. Li, Q. Chen, Recent advances toward practical use of halide perovskite nanocrystals, J. Mater. Chem. A 6 (2018) 21729–21746, https://doi.org/10.1039/C8TA06376A.

[3] F. Zhang, J. Song, T. Fang, B. Han, H. Zeng, J. Li, High-efficiency pure-color inorganic halide perovskite emitters for ultrahigh-definition displays: progress for backlighting displays and electrically driven devices, Small Methods 2 (2018) 1700382, https://doi.org/10.1002/smtd.201700382.

[4] H.C. Yoon, H. Kang, S. Lee, J.H. Oh, H. Yang, Y.R. Do, Study of perovskite QD down-converted LEDs and six-color white LEDs for future displays with excellent color performance, ACS Appl. Mater. Interfaces 8 (2016) 18189–18200, https://doi.org/10.1021/acsami.6b05468.

[5] Q.A. Akkerman, V. D'Innocenzo, S. Accornero, A. Scarpellini, A. Petrozza, M. Prato, L. Manna, Tuning the optical properties of cesium lead halide perovskite nanocrystals by anion exchange reactions, J. Am. Chem. Soc. 137 (2015) 10276–10281, https://doi.org/10.1021/jacs.5b05602.

[6] C.C. Lin, A. Meijerink, R.S. Liu, Critical red components for next-generation white LEDs, J. Phys. Chem. Lett. 7 (2016) 495–503, https://doi.org/10.1021/acs.jpclett.5b02433.

[7] M.J. Grotevent, M.V. Kovalenko, M.I. Bodnarchuk, L. Protesescu, G. Nedelcu, S. Yakunin, Fast anion-exchange in highly luminescent nanocrystals of cesium lead halide perovskites (CsPbX 3, X = Cl, Br, I), Nano Lett. 15 (2015) 5635–5640, https://doi.org/10.1021/acs.nanolett.5b02404.

[8] J. Zhou, Z. Hu, L. Zhang, Y. Zhu, Perovskite CsPbBr 1.2I1.8quantum dot alloying for application in white light-emitting diodes with excellent color rendering index, J. Alloys Compd. 708 (2017) 517–523, https://doi.org/10.1016/j.jallcom.2017.03.043.

[9] S.H. Choi, J.S. Yoo, Y.H. Song, H.S. Jung, E.K. Ji, D.H. Yoon, B.K. Kang, Design of long-term stable red-emitting CsPb(Br 0.4, I 0.6) 3 perovskite quantum dot film for generation of warm white light, Chem. Eng. J. 313 (2016) 461–465, https://doi.org/10.1016/j.cej.2016.12.087.

[10] W. Lu, B. Zou, H. Zhong, Q. Zhou, Z. Bai, Y. Wang, In situ fabrication of halide perovskite nanocrystal-embedded polymer composite films with enhanced photoluminescence for display backlights, Adv. Mater. 28 (2016) 9163–9168, https://doi.org/10.1002/adma.201602651.

[11] S. Pathak, N. Sakai, F. Wisnivesky, S.D. Rocca Rivarola, J. Stranks, G.E. Liu, C. Eperon, K. Ducati, J.T. Wojciechowski, A.A. Griffiths, A. Haghighirad, R.H. Pellaroque, H.J Snaith Friend, Perovskite crystals for tunable white light emission, Chem. Mater. 27 (2015) 8066–8075, https://doi.org/10.1021/acs.chemmater.5b03769.

[12] X. Di, J. Jiang, Z. Hu, L. Zhou, P. Li, S. Liu, W. Xiang, X. Liang, Stable and brightly luminescent all-inorganic cesium lead halide perovskite quantum dots coated with mesoporous silica for warm WLED, Dye. Pigment. 146 (2017) 361–367, https://doi.org/10.1016/j.dyepig.2017.07.028.

[13] H. Shao, X. Bai, G. Pan, H. Cui, J. Zhu, Y. Zhai, J. Liu, B. Dong, L. Xu, H. Song, Highly efficient and stable blue-emitting CsPbBr 3@SiO2 nanospheres through low temperature synthesis for nanoprinting and WLED, Nanotechnology 29 (2018), https://doi.org/10.1088/1361-6528/aac00b.

[14] M.S. Onses, E. Sutanto, P.M. Ferreira, A.G. Alleyne, J.A. Rogers, Mechanisms, capabilities, and applications of high-resolution electrohydrodynamic jet printing, Small 11 (2015) 4237–4266, https://doi.org/10.1002/smll.201500593.

[15] M.S. Onses, A. Ramírez-Hernández, S.M. Hur, E. Sutanto, L. Williamson, A.G. Alleyne, P.F. Nealey, J.J. De Pablo, J.A. Rogers, Block copolymer assembly on nanoscale patterns of polymer brushes formed by electrohydrodynamic jet printing, ACS Nano 8 (2014) 6606–6613, https://doi.org/10.1021/nn5022605.

[16] N.B. Kiremitler, S. Pekdemir, J. Patarroyo, S. Karabel, I. Torun, V.F. Puntes, M.S. Onses, Assembly of plasmonic nanoparticles on nanopatterns of polymer brushes fabricated by electrospin nanolithography, ACS Macro Lett. 6 (2017) 603–608, https://doi.org/10.1021/acsmacrolett.7b00288.

[17] L. Williamson, P.F. Nealey, H. Ahn, M.S. Onses, C. Song, J.A. Rogers, P.M. Ferreira, E. Sutanto, A.G. Alleyne, Hierarchical patterns of three-dimensional block-copolymer films formed by electrohydrodynamic jet printing and self-assembly, Nat. Nanotechnol. 8 (2013) 667–675, https://doi.org/10.1038/nnano.2013.160.

[18] J. Schneider, P. Galliker, D. Poulikakos, V. Sandoghdar, H. Eghlidi, S. Kress, Direct printing of nanostructures by electrostatic autofocussing of ink nanodroplets, Nat. Commun. 3 (2012) 890–899, https://doi.org/10.1038/ncomms1891.

[19] S.J.P. Kress, P. Galliker, D.K. Kim, S.V. Jayanti, P. Richner, D.J. Norris, D. Poulikakos, Near-field light design with colloidal quantum dots for photonics and plasmonics, Nano Lett. 14 (2014) 5827–5833, https://doi.org/10.1021/nl5026997.

[20] J.A. Rogers, N.H. Kim, J. Lee, K.J. Yu, J. Bin Lim, N. Oh, B.H. Kim, S.-K. Kang, C. Leal, M. Shim, H. Kim, M.S. Onses, J.W. Lee, S. Nam, J.-H. Kim, C.H. Lee, J.H. Shin, High-resolution patterns of quantum dots formed by electrohydrodynamic jet printing for light-emitting diodes, Nano Lett. 15 (2015) 969–973, https://doi.org/10.1021/nl503779e.

[21] J. De Roo, M. Ibáñez, P. Geiregat, G. Nedelcu, W. Walravens, J. Maes, J.C. Martins, I. Van Driessche, M.V. Kovalenko, Z. Hens, Highly dynamic ligand binding and light absorption coefficient of cesium lead bromide perovskite nanocrystals, ACS Nano. 10 (2016) 2071–2081, https://doi.org/10.1021/acsnano.5b06295.

[22] S. Dadı, Y. Altıntas, E. Beskazak, E. Mutlugun, Plasmon enhanced emission of perovskite quantum dot films, MRS Adv. 3 (2018) 733–739, https://doi.org/10.1557/adv.2018.6.

[23] M. Grabolle, M. Spieles, V. Lesnyak, N. Gaponik, A. Eychmüller, U. Resch-Genger, Determination of the fluorescence quantum yield of quantum dots: suitable procedures and achievable uncertainties, Anal. Chem. 81 (2009) 6285–6294, https://doi.org/10.1021/ac900308v.

[24] Y. Altintas, M.Y. Talpur, E. Mutlugün, Cd-free quantum dot pellets for efficient white light generation, Opt. Express. 25 (2017), https://doi.org/10.1364/OE.25.028371.

[25] Y. Altintas, N.B. Kiremitler, S. Genc, M.S. Onses, E. Mutlugün, FRET enabled light harvesting within quantum dot loaded nanofibers, J. Phys. D. Appl. Phys. 51 (2018), https://doi.org/10.1088/1361-6463/aaa55a.

[26] Y. Bekenstein, B.A. Koscher, S.W. Eaton, P. Yang, A.P. Alivisatos, Highly luminescent colloidal nanoplates of perovskite cesium lead halide and their oriented assemblies, J. Am. Chem. Soc. 137 (2015) 16008–16011, https://doi.org/10.1021/jacs.5b11199.

[27] K. Barton, S. Mishra, K. Alex Shorter, A. Alleyne, P. Ferreira, J. Rogers, A desktop electrohydrodynamic jet printing system, Mechatronics 20 (2010) 611–616, https://doi.org/10.1016/j.mechatronics.2010.05.004.

[28] N. Mondal, A. De, A. Samanta, Achieving near-unity photoluminescence efficiency for blue-violet-emitting perovskite nanocrystals, ACS Energy Lett. 4 (2019) 32–39, https://doi.org/10.1021/acsenergylett.8b01909.

[29] T. Erdem, H.V. Demir, Color science of nanocrystal quantum dots for lighting and displays, Nanophotonics 2 (2013), https://doi.org/10.1515/nanoph-2012-0031.

[30] T. Erdem, S. Nizamoglu, X.W. Sun, H.V. Demir, A photometric investigation of ultra-efficient LEDs with high color rendering index and high luminous efficacy employing nanocrystal quantum dot luminophores, Opt. Express. 18 (2010), https://doi.org/10.1364/OE.18.000340.

[31] I. Torun, Y. Altintas, A.F. Yazici, E. Mutlugun, M.S. Onses, Solid-state encapsulation and color tuning in films of cesium lead halide perovskite nanocrystals for white light generation, ACS Appl. Nano Mater. 2 (2019) 1185–1193, https://doi.org/10.1021/acsanm.8b02030.

[32] S. Nizamoglu, T. Erdem, X.W. Sun, H.V. Demir, Warm-white light-emitting diodes integrated with colloidal quantum dots for high luminous efficacy and color rendering: reply to comment, Opt. Lett. 36 (2011), https://doi.org/10.1364/OL.36.002852.

[33] E. Sutanto, K. Shigeta, Y.K. Kim, P.G. Graf, D.J. Hoelzle, K.L. Barton, A.G. Alleyne, P.M. Ferreira, J.A. Rogers, A multimaterial electrohydrodynamic jet (E-jet) printing system, J. Micromech. Microeng. 22 (2012) 45008, https://doi.org/10.1088/0960-1317/22/4/045008.

[34] T. Erdem, S. Nizamoglu, H.V. Demir, Computational study of power conversion and luminous efficiency performance for semiconductor quantum dot nanophosphors on light-emitting diodes, Opt. Express. 20 (2012) 3275–3295.